SCIENTIFIC REPORTS

OPEN

The double solid solution (Zr, Nb)$_2$(Al, Sn)C MAX phase: a steric stability approach

Thomas Lapauw[1,2], Bensu Tunca[1,2], Daniel Potashnikov[3], Asaf Pesach[4], Offir Ozeri[5], Jozef Vleugels[1] & Konstantina Lambrinou[2]

The addition of Nb and Sn to Zr$_2$AlC is investigated, targeting the synthesis of a Zr-rich bulk MAX phase free of ZrC. The 211 phase formation in the two quaternary Zr-Nb-Al-C and Zr-Al-Sn-C systems is evaluated. Solubility over the entire compositional range in (Zr, Nb)$_2$AlC and Zr$_2$(Al, Sn)C is observed. In terms of effectiveness, the addition of Sn is preferred over the addition of Nb, as the former is selectively incorporated into the 211 structure. A combinatorial approach results in the formation of phase-pure (Zr$_{0.8}$, Nb$_{0.2}$)$_2$(Al$_{0.5}$, Sn$_{0.5}$)C. The effect of the added solutes on the microstructure and crystallographic parameters is investigated. The addition of Nb and Sn reduces the distortion parameter of the trigonal prism compared to pure Zr$_2$AlC. Therefore, an attempt is made to establish a more general stability criterion for the M$_2$AC structure based on the steric relationship between the atoms in the M$_6$A trigonal prism. Inspired by the Hume-Rothery rules, it is suggested that comparable atomic radii of the M- and A-atoms provide a good starting point to obtain a stable 211 MAX phase.

A group of layered ternary carbides and nitrides, commonly known as the MAX phases, is studied intensively in the last 20 years due to their remarkable set of properties[1,2]. The M$_{n+1}$AX$_n$ phases, where M is an early transition metal, A is an element from groups 12–15 in the periodic table, X is C and/or N and n is an integer commonly equal to 1, 2 or 3 (forming subgroups 211 – earlier referred to as the H-phases[2], 312 and 413, respectively), combine the properties of ceramics with some merits of metals. These properties result from their laminated nature, as n M$_6$X octahedra are alternated with atomic layers of A[3,4].

Recently, the interest in Zr-based MAX phase carbides (Zr$_{n+1}$AC$_n$) arose, mainly triggered by their potential use in the nuclear sector. Zr is the preferred M-element as it has a small neutron cross-section for thermal and fast neutrons[5], Al offers the potential of forming a protective Al$_2$O$_3$ layer in oxidative environments. C is preferred over N as X-element in order to avoid the production of the long-lived ^{14}C radioisotope during irradiation. More specifically, Zr-based MAX phases are considered candidate coating materials for the protection of Zr-based alloy fuel clads designed to increase the accident tolerance of Gen-II/III LWRs (light water reactors)[6]. Alternatively, select MAX phases in bulk (monolithic) form are considered as structural materials for pump impellers intended for use in Gen-IV LFRs (lead-cooled fast reactors)[7]. This component is exposed to fast-flowing lead-based alloys, i.e., conditions in which conventional nuclear steel grades may suffer erosion/corrosion that leads to severe material loss[8].

Although the ternary Zr$_2$AlC phase could be synthesized, the material contained a significant amount of the undesirable ZrC phase, making the synthesis of phase-pure Zr$_2$AlC MAX phase materials very challenging[9,10]. An alternative approach to obtain MAX phase pure material is to stabilize this stoichiometry by making (Zr, M)$_2$AlC and Zr$_2$(Al, A)C solid solutions[11]. Stable solid solutions on the M-site have been reported for M = Nb and Ti[12–14], while recently the in-plane ordered (V$_{2/3}$, Zr$_{1/3}$)$_2$AlC i-MAX phase was synthesized[15]. Horlait *et al.* successfully substituted Al with Sn, Pb, Sb and Bi[11,16]. However, ZrC or (Zr, M)C was reported as parasitic phase in all Zr$_2$AlC-based solid solutions. In order to fully benefit from the aforementioned unique set of MAX phase properties, elimination of this high hardness, rock-salt-structured carbide phase is desired. Only when this is

[1]KU Leuven, Department of Materials Engineering, Kasteelpark Arenberg 44, B-3001, Leuven, Belgium. [2]SCK•CEN, Boeretang 200, B-2400, Mol, Belgium. [3]Israel Atomic Energy Commission, P.O. Box 7061, Tel-Aviv, 61070, Israel. [4]Physics Department, Nuclear Research Centre – Negev, Beer-Sheva, 84190, Israel. [5]Reactor Department, Nuclear Research Center-Soreq, Yavne, 81800, Israel. Correspondence and requests for materials should be addressed to T.L. (email: thomas.lapauw@kuleuven.be)
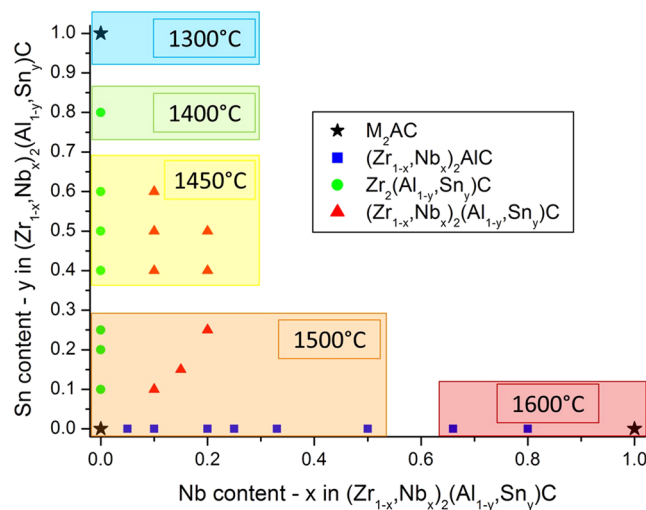
Figure 1. The various $(Zr_{1-x}, Nb_x)_2(Al_{1-y}, Sn_y)C$ compositions synthesised in this study. The temperature refers to the synthesis temperature during reactive hot pressing.

realised, the phase-pure material properties can be experimentally determined, allowing the exploitation of the full potential of these ternary ceramics for select applications in the nuclear field.

This work aims to synthesise a material, which contains only Zr_2AlC-based MAX phases and is free from NaCl-structured carbides, like ZrC. Nb and Sn are selected as alloying elements on the M- and A-site, respectively, targeting a double solid solution with the $(Zr_{1-x}, Nb_x)_2(Al_{1-y}, Sn_y)C$ general stoichiometry. The effect of these alloying elements on the crystal structure are evaluated.

Methods

Synthesis.   Ceramic disks were synthesised via a powder metallurgical route. Starting powders of ZrH_2 ($<6\,\mu m$, Rockwood Lithium), $NbH_{0.89}$ ($<40\,\mu m$, CBMM), Al ($<5\,\mu m$, AEE), Sn ($<5\,\mu m$, AEE) and C ($<5\,\mu m$, Asbury) were mixed in a near-stoichiometric ratio M:A:X = 2:1.1:0.95. A slight excess of the A-element was added to compensate for losses during sintering, while a substoichiometric amount of X compensated for the inward C diffusion from the graphitic sintering environment. In total 27 different ceramics were prepared with different Zr:Nb and Al:Sn ratios, as summarised in Fig. 1. Composition-wise, the produced ceramics can be divided in 4 groups: (1) M_2AC ternary compounds that served as reference materials; (2) $(Zr_{1-x}, Nb_x)_2AlC$ and (3) $Zr_2(Al_{1-y}, Sn_y)C$ quaternary compounds; and (4) the double solid solutions $(Zr_{1-x}, Nb_x)_2(Al_{1-y}, Sn_y)C$ (quinary compounds). Since Zr-rich MAX phases are of primary interest, the amount of Nb in the double solid solution is limited to 20 at% on the M-site (i.e., x = 0.2).

The different powder mixtures were prepared in isopropanol using a multidirectional mixer (Turbula, WAB, Switzerland) for 24 h. The dried powders were pre-compacted at 30 MPa in a graphite die (Ø 30 mm) and densified by reactive hot-pressing (W100/150-2200-50 LAX, FCT Systeme, Frankenblick, Germany) in an actively maintained vacuum (10 Pa). The green powder compacts were heated at 20 °C/min under a load of 7 MPa up to the final synthesis temperature, which was composition-dependent, ranging from 1300 °C for Zr_2SnC (~1250 °C)[17], through 1500 °C for Zr_2AlC (~1525 °C)[9], to 1600 °C for Nb_2AlC (1600 °C)[18]. Other temperatures were used for mixed compositions (i.e., with more than 3 elements). The sintering temperature for each composition is given in Fig. 1. Upon reaching the sintering temperature, the pressure was increased to 30 MPa and was maintained constant during a dwell time of 60 min. The M:A-ratio in the starting powder was adjusted to 2:1.05, in order to minimize the formation of intermetallic phases. After sintering, the surfaces of the ceramic discs were ground in order to remove the C-rich outer layer.

Characterisation.   X-ray diffraction (XRD) was used to identify and analyse the phase assembly in the sintered ceramic discs. The diffraction patterns were obtained using Cu K_α radiation in a Bragg-Brentano geometry. The diffractometer (Bruker D2) was operated at room temperature, at 30 kV and 10 mA. Measurements were performed in the 5° to 75° 2θ range with a step size of 0.02° 2θ and 0.2 s per step. Rietveld refinement was carried out using the Materials Analysis Using Diffraction (MAUD) software[19]. The a and c lattice parameters (LPs) were determined on the sintered discs with an accuracy of 10^{-3} Å and 5×10^{-3} Å, respectively. The line-broadening and size-strain model used for the refinement were based on the Popa rules[20]. The microstructure of mirror-polished ceramics was characterized with scanning electron microscopy (SEM; XL30-FEG, FEI, The Netherlands) equipped with an energy dispersive X-ray spectrometer (EDS; EDAX). Neutron powder diffraction (NPD) was carried out on Zr_2SnC powder that was produced by ring milling (Retsch RS200) a piece of the respective hot-pressed disc during 1 min at 1000 rpm. The diffraction experiments were carried out with the KARL double axis diffractometer[21], mounted on the Israeli Research Reactor 1. The measurement was performed using similar conditions as those used previously for Zr_2AlC[9]. The NPD data were analyzed using the Rietveld refinement method, applied within the FullProf software.
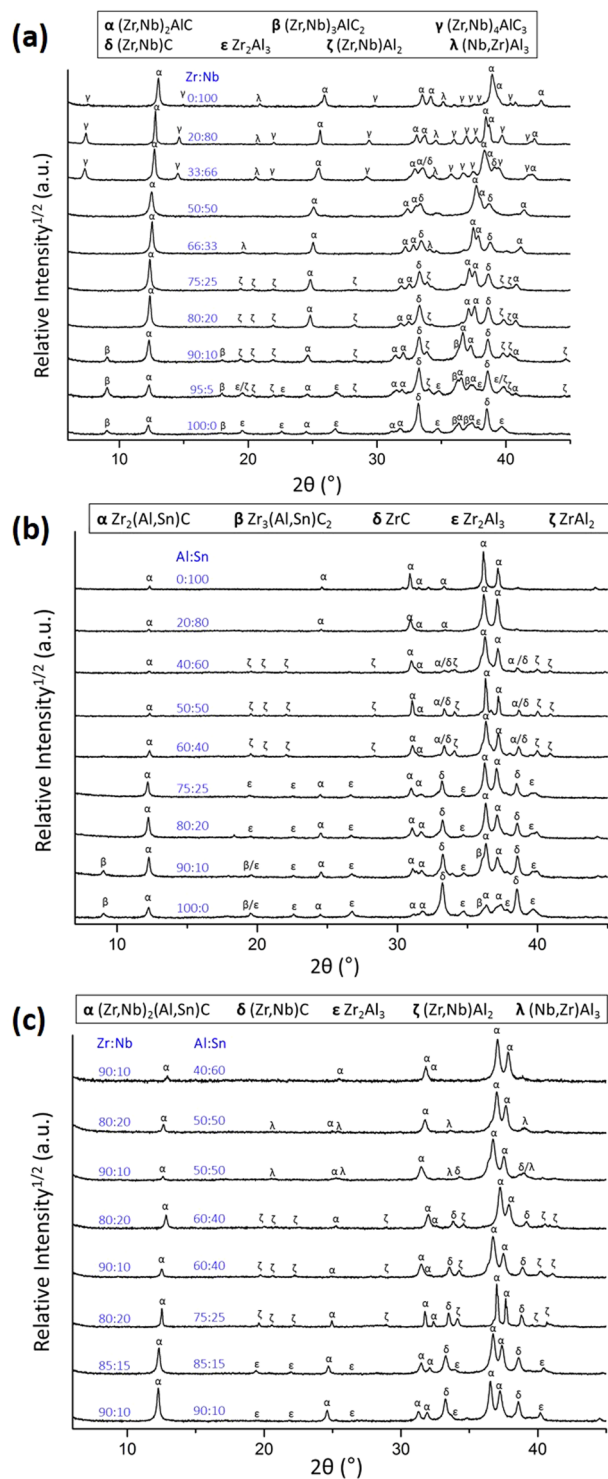
Figure 2. XRD patterns of the (**a**) $(Zr_{1-x}, Nb_x)_2Al_{1.1}C_{0.95}$ ceramics, (**b**) $Zr_2(Al_{1-y}, Sn_y)_{1.1}C_{0.95}$ ceramics and (**c**) $(Zr_{1-x}, Nb_x)_2(Al_{1-y}, Sn_y)_{1.1}C_{0.95}$ double solid solution ceramics.

Results

$(Zr, Nb)_2AlC$. First, the effect of adding Nb as alloying element was investigated. Figure 2a shows the XRD patterns of ceramics with a $(Zr_{1-x}, Nb_x)_2Al_{1.1}C_{0.95}$ starting composition (the refined XRD patterns are included in the Supporting Information). The main diffraction peaks of the constituent phases are identified, mainly corresponding to $(Zr, Nb)_2AlC$ and $(Zr, Nb)C$. The relative intensity of the $(Zr, Nb)C$ peaks decreased with increasing Nb-content and this parasitic phase was completely absent at $x = 0.8$. At higher Nb-content ($x \geq 0.66$), a fraction of $(Nb, Zr)_4AlC_3$ was observed, whereas the peaks of the 312 MAX phase could be identified at low Nb-content ($x \leq 0.1$). Apart from the carbide phases, some secondary intermetallics were present, i.e., $(Zr, Nb)Al_2$ and Zr_2Al_3
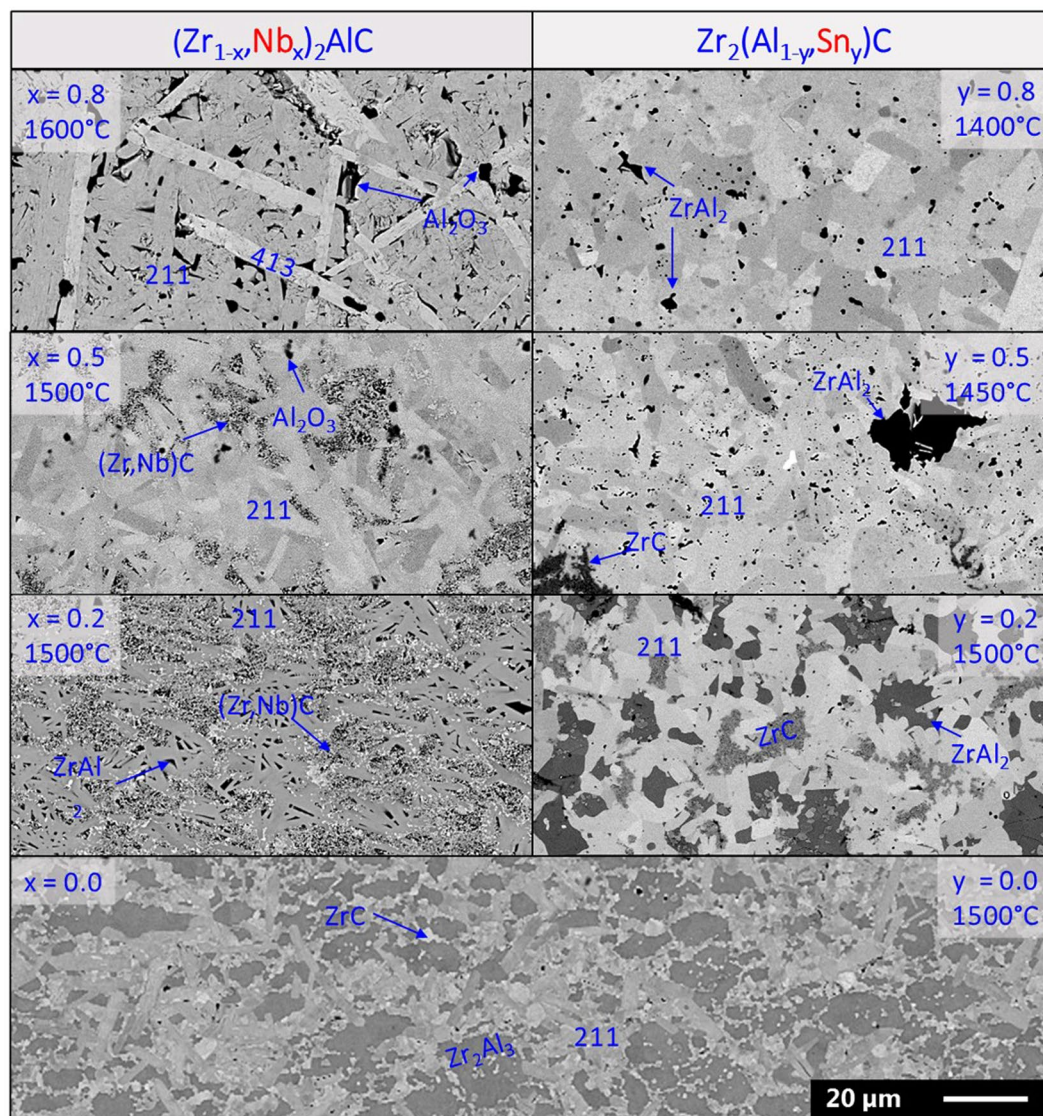
Figure 3. BSE micrographs of $(Zr_{1-x}, Nb_x)_2Al_{1.1}C_{0.95}$ and $Zr_2(Al_{1-y}, Sn_y)_{1.1}C_{0.95}$ ceramics with varying Nb-content (left) and Sn-content (right). The scale bar in the lower right corner is valid for all micrographs.

at low Nb-content and $(Nb, Zr)Al_3$ in the Nb-rich ceramics. It is important to note that some of the parasitic phases can form (Zr, Nb)-based substitutional solid solutions. For example, $(Zr_{1-x}, Nb_x)C$ has been reported as stable over the entire compositional range ($0 \leq x \leq 1$) above 570 °C[22]. The solubility ranges reported at 925 °C for $(Zr_{1-x}, Nb_x)Al_2$ and $(Nb_{1-x}, Zr_x)Al_3$ correspond to $x = 0.15$ and $x = 0.68$, respectively[23]. This indicates that alloying with Nb did not selectively favour the stabilization of the 211 MAX phase structure, and Nb was also incorporated in the competing parasitic phases.

The change in phase content was also reflected in the microstructure. The backscattered electron detector (BSE) micrographs of the $(Zr_{1-x}, Nb_x)_2AlC$ ceramics with different Nb-content ($x = 0$, 0.2, 0.5 and 0.8) are compared in the left column of Fig. 3. The elongated grains correspond to MAX phase grains, the volume fraction of which increased with increasing Nb-content. For $x = 0$, the relatively small grains of the 211 MAX phase are surrounded by Zr_2Al_3 regions with interspersed μm-sized ZrC particles. By adding Nb ($x = 0.2$ and 0.5), the (Zr, Nb)C grain size was significantly refined, a fact that could be attributed to a partial decomposition of the $(Zr, Nb)_2AlC$ into NbC and ZrC during cooling (<570 °C)[22]. Isolated Al_2O_3 particles were present at higher Nb-content ($x = 0.5$ and 0.8). These formed during the aluminothermic reduction of Nb_2O_5 that was present in the Nb-starting powder. Furthermore, 413 MAX phase grains can be distinguished at $x = 0.8$.

The a and c LPs of $(Zr, Nb)_2AlC$ are shown in Fig. 4a,b, respectively, and some of them are included in Table 1 (blue squares). The relative value on the secondary (right) y-axis is a comparison with the LPs of Zr_2AlC. A linear decrease of both a and c LPs with increasing Nb-content was observed resulting in a clear lattice shrinkage. This linear trend is in agreement with Vegard's law, suggesting that $(Zr, Nb)_2AlC$ forms a solid solution over the entire compositional range. The shrinkage was caused by the smaller atomic radius of Nb as compared to Zr, an effect that was also observed in $(Nb, Zr)_4AlC_3$[24]. However, despite the fact that the starting powder was

Sn-y	0			0.4			0.5			0.6		
Nb-x		a (Å)	c (Å)		a (Å)	c (Å)		a (Å)	c (Å)		a (Å)	c (Å)
0	★	3.324	14.571	●	3.338	14.576	●	3.345	14.577	●	3.349	14.579
0.1	■	3.296	14.508	▲	3.316	14.518	▲	3.324	14.523	▲	3.327	14.527
0.2	■	3.267	14.451	▲	3.290	14.460	▲	3.295	14.464		—	—

Table 1. A subset of the a and c LPs for the 211 phases in $(Zr_{1-x}, Nb_x)_2(Al_{1-y}, Sn_y)_{1.1}C$ ceramics, as determined from XRD (Fig. 2). The uncertainty on the experimentally obtained LPs is in the range of $\pm 10^{-3}$ Å. The coloured symbols correspond to those used in Fig. 1.
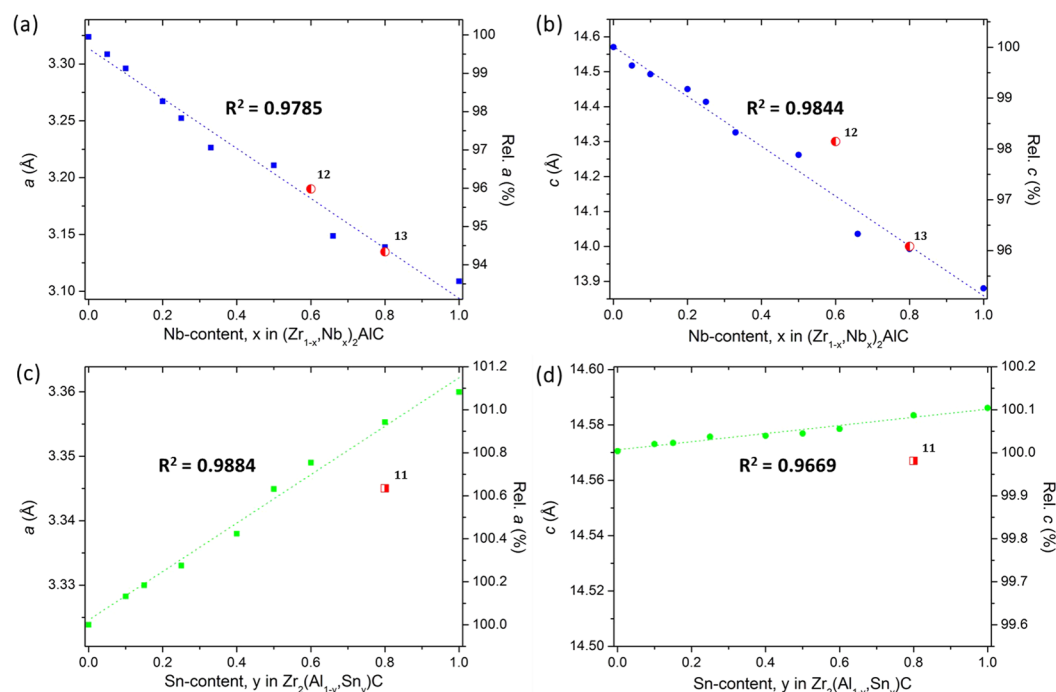
Figure 4. The evolution of the a and c LPs with the addition of Nb (**a,b**) and Sn (**c,d**).

near-stoichiometric, synthesis of phase-pure materials was difficult as the rock-salt-structured (Zr, Nb)C was always present in the Zr-rich compositions, disappearing only at a high Nb-content (x = 0.8).

Two reports on $(Zr, Nb)_2AlC$ are available in literature. In 1966, Reiffenstein could substitute Nb by Zr in a Nb/Zr ratio of 1.5 or equivalently synthesise $(Zr_{0.4}, Nb_{0.6})_2AlC$, starting from Nb_2AlC[12]. However, no further information on the starting composition or additional phases was provided. More recently, Naguib reported on various solid solutions and the formation of $(Zr_{0.2}, Nb_{0.8})_2AlC$, starting from a Zr:Nb ratio of 25:75, with about 9 wt% of ZrC and a minor amount of Zr_5Al_3[13]. The reported LPs are included in red in Fig. 4a,b and fit the suggested trend line. The outlier for the c-value of $(Zr_{0.4}, Nb_{0.6})_2AlC$ might be attributed to its large uncertainty, which was reported to be 14.3 ± 0.7 Å[12]. Overall, it is clear that the addition of Nb promotes the formation of the 211 MAX phase in the Zr-Nb-Al-C system and lowers the relative stability of (Zr, Nb)C as compared with the (Zr, Nb)$_2$AlC phase. However, the required Nb-content to obtain phase-pure MAX phase materials is high (x > 0.66).

$Zr_2(Al, Sn)C$. Second, the effect of adding Sn as alloying element was investigated and Fig. 2b shows the XRD patterns of the produced $Zr_2(Al_{1-y}, Sn_y)_{1.1}C_{0.95}$ ceramics (the refined XRD patterns are included in the Supporting Information). Similarly as in the addition of Nb, the rock-salt-structured ZrC was the main competing phase. A small fraction of the 312 MAX phase was observed at low Sn-content (y ≤ 0.1). For y ≤ 0.25, the Zr_2Al_3 intermetallic compound was detected, whereas $ZrAl_2$ was found in the ceramics with higher Sn-content. In contrast with the Nb substitution, the competing phases do not form a notable solid solution with Sn and, thus, this alloying element was selectively incorporated into $Zr_2(Al, Sn)C$. This results in an effective stabilization of the 211 MAX phase, which was nearly phase-pure at y = 0.6, with 4 wt% ZrC and 9 wt% $ZrAl_2$. $ZrAl_2$ was mainly present due to the superstoichiometric amounts of A-elements (Al and Sn) in the starting powder (M:A = 2:1.1), which resulted in the formation of a $Zr_2(Al_{0.34}, Sn_{0.66})C$ solid solution, as Sn was exclusively dissolved in the MAX phase and the leftover Al formed $ZrAl_2$. The XRD patterns were used to calculate the LPs, the evolution of a and c with the Sn-content in the starting powder is shown in Fig. 4c,d, respectively, and some of the data are included in Table 1

(green dots). A good fit with the linear trend of Vegard's law was obtained by assuming that Sn can substitute Al over the entire compositional range. The *a* values for the high-Sn-containing ceramics (y = 0.5, 0.6 and 0.8) were slightly above the linear trend, due to the superstoichiometric ratio of A in the starting powder, and the resulting MAX phase composition corresponds roughly to $Zr_2(Al_{0.45}, Sn_{0.55})C$, $Zr_2(Al_{0.34}, Sn_{0.66})C$ and $Zr_2(Al_{0.12}, Sn_{0.88})C$, respectively. The substitution of Sn caused an expansion of the unit cell, mainly due to an increase in the *a*-LP, whereas *c* remained almost constant with only a relative difference of 0.1% between Zr_2AlC and Zr_2SnC. This was also observed by Horlait *et al.* for $Zr_2(Al, A)C$ with A = Sn and other heavy A-elements, such as Pb, Sb and Bi[11]. The values reported for $Zr_2(Al_{0.2}, Sn_{0.8})C$ are included in Fig. 4c,d. Both parameters are lower compared to the observed trend in this study. However, the differences are small, i.e., <0.4% for *a* and <0.05% for *c*, which can be attributed to local variations in composition.

The microstructure of the produced $Zr_2(Al_{1-y}, Sn_y)_{1.1}C_{0.95}$ ceramics for y = 0, 0.2, 0.5 and 0.8 is shown in the right column of Fig. 3. The three constituent phase types are indicated on the images. With increasing Sn-content, the ZrC and intermetallic phase (Zr_2Al_3 and $ZrAl_2$) fractions clearly decreased. These intermetallics are present as separate patches between the MAX phase grains. This morphology differs from the $(Zr_{1-x}, Nb_x)_2AlC$ micro-structure, where the intermetallics mainly act as binder for the finely dispersed (Zr, Nb)C. Also the morphology of the MAX grains changed with the added element. The platelet shape was more pronounced when Nb was added, whereas the addition of Sn resulted in more equiaxed grains. It is inferred that the observed difference in anisotropic grain growth reflects differences in the *c/a*-ratio, which decreased from 4.465 for Nb_2AlC, through 4.384 for Zr_2AlC, to 4.341 for Zr_2SnC.

(Zr, Nb)$_2$(Al, Sn)C. Thirdly, the effect of adding both Nb and Sn was investigated and the XRD patterns of the 8 produced $(Zr_{1-x}, Nb_x)_2(Al_{1-y}, Sn_y)_{1.1}C_{0.95}$ ceramics are compared in Fig. 2c (the refined XRD patterns are included in the Supporting Information). The amount of Nb added to the double solid solutions was limited to x ≤ 0.2 for three reasons: (1) the main interest is in Zr-based MAX phases due to their small neutron cross-section, (2) taking into account the observations made for the two pseudo-ternary systems, where Nb can be incorporated in the competing phases while Sn is selectively only present in the 211 MAX phase, and (3) Nb-rich MAX phases are known to have a poor oxidation resistance[25].

Analysing the evolution of the phase content, a similar trend as for the quaternary systems was found. Adding Nb and Sn to the Zr-Al-C system increased the fraction of the 211 MAX phase and no parasitic (Zr, Nb)C phase was observed for the combinations of Zr:Nb & Al:Sn equal to 80:20 & 50:50 and 90:10 & 40:60. This observation is supported by the microstructural evolution, as shown in Fig. 5. At lower Sn substitution levels, (Zr, Nb)C was always present with an intermetallic compound to accommodate the Al surplus. The intermetallic compound evolved with increasing Sn-content from Zr_2Al_3 (y ≤ 0.15), through (Zr, Nb)Al$_2$ (0.25 ≤ y ≤ 0.4), to (Nb, Zr)Al$_3$ (y = 0.5).

In order to avoid the formation of these intermetallic phases, the M:A-ratio in the starting powder was adjusted from 2:1.10 to 2:1.05 at a later stage of this study. This difference in M:A-ratio is indeed clearly reflected in the microstructure of the two ceramics with x = 0.2 and y = 0.5 shown in Fig. 5. The *a* and *c* LPs for some of the double solid solutions are included in Table 1 (red triangles). The trends for the *a* and *c* LPs are the same as those observed in the quaternary systems. An increase in Sn-content results mainly in an increased *a*-LP, whereas *c* increases only slightly. The addition of Nb decreases both LPs. These trends are further investigated in the next section, which attempts to correlate the *a* and *c* LPs with the stability of the 211 MAX phases.

Discussion

It is clear that the addition of Nb and/or Sn to the starting powder increases the phase stability of the 211 MAX phases, as compared to the stability of the competing binary carbide ZrC. The reason for this, as inspired by Hägg's rule for binary carbides[26], might be found in the way these elements alter the crystallographic parameters and concomitantly sterically stabilize the MAX phase structure. In the M_2AX phase structure (Fig. 6a), there are 3 free variables determining the unit cell: *a*, *c* and the relative z-coordinate of the M-atom, z_M. The latter defines the height of the M-atoms above the layer of C or N, and varies commonly in the 0.08–0.09 range. Obviously, z_M directly affects the distance between the M and X atoms, d_{M-X}:

$$d_{M-X} = \sqrt{\frac{a^2}{3} + (cz_M)^2}$$

(1)

As may be seen from the schematic representation of the 211 MAX phase structure in Fig. 6a, the unit cell can be considered as an alternating stack of M_6X-octahedra, indicated in orange, and M_6A-triangular prisms, indicated in red. A similar representation of the crystal structure is valid for the other common MAX phase types, 312 and 413, with a building block of 2 and 3 M_6X-octahedra interleaving the M_6A-layers, respectively.

For the binary NaCl-structured MX phase, the unit block consists of a cubic octahedron with fourfold symmetry axes. In the case of M_2AX, however, the octahedral block is not ideally cubic, resulting in a reduced symmetry. This distortion can be quantified by the distortion parameter, o_d, which is the ratio of distances between two octahedral faces off the basal plane (d_1) and two octahedral faces in the basal plane (d_2)[27]. These distances are indicated in Fig. 6a and are measured on the octahedral faces, as defined by the projections in Fig. 6b. The ratio corresponds to[27]:

$$o_d = \frac{d_1}{d_2} = \frac{\sqrt{3}}{2\sqrt{4z_M^2\left(\frac{c}{a}\right)^2 + \frac{1}{12}}}$$

(2)
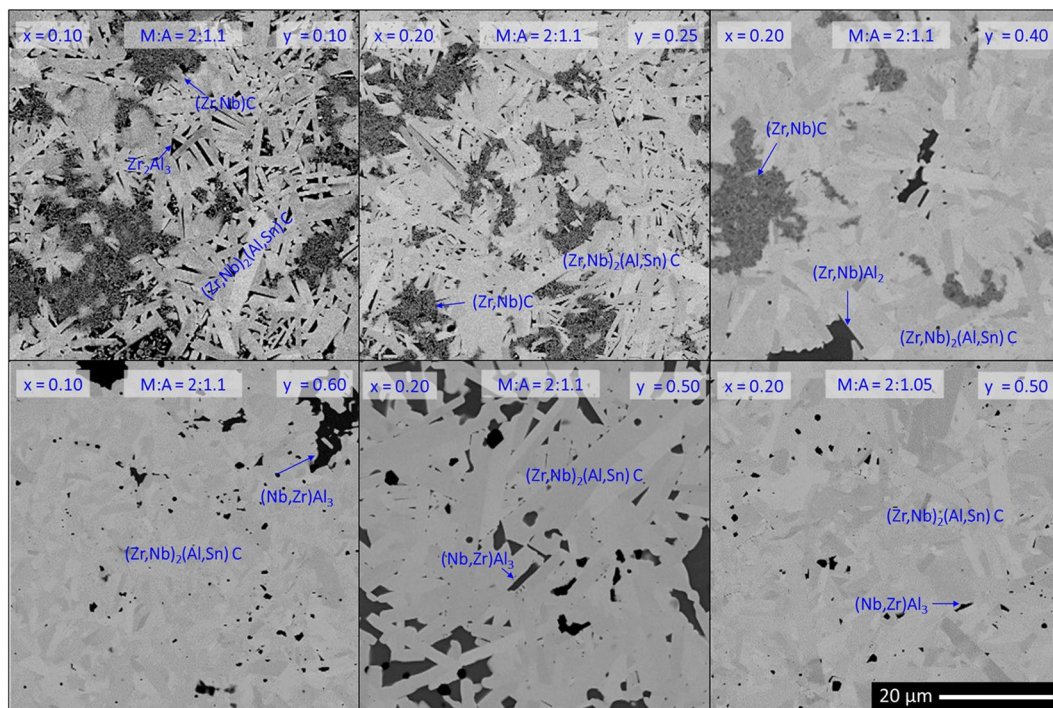
Figure 5. BSE micrographs of various $(Zr_{1-x}, Nb_x)_2(Al_{1-y}, Sn_y)C$-based double solid solutions. The scale bar in the lower right corner is valid for all micrographs.
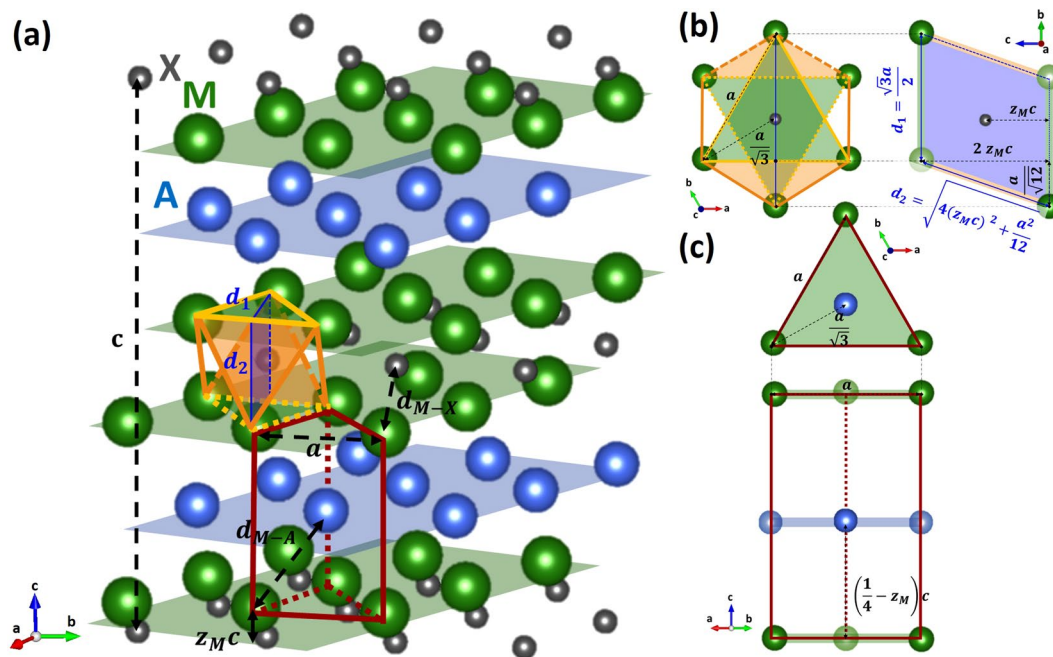
Figure 6. The crystallographic parameters as defined for M_2AX with (**a**) the 3D-structure with the M_6X octahedron indicated in orange and the M_6A trigonal prism indicated in red; (**b**) the projected octahedron; and (**c**) the projected trigonal prism.

In the 211 MAX phase structure, the distortion is influenced by c/a and z_M. o_d becomes equal to 1 for a perfect cubic octahedron, which would assume ideal, close-packed spheres ($c/a = 2\sqrt{6} \approx 4.89$) and the M-atom at the canonical position ($z_M = 1/12 \approx 0.0833$). Typically, the values reported for o_d are >1, indicating a compression of the octahedron block along the c-axis.

MAX Phase	c/a	z_M	d_{M-A}	d_{M-X}	o_d	p_d	Method	Ref.
ideal hcp spheres	$2\sqrt{6} \approx 4.89$	$1/12 \approx 0.0833$	—	—	1	1	—	—
Ti$_2$GaC	4.349	0.0865	2.817	2.120	1.074	1.092	SC-XRD	[33]
Cr$_2$GaC	4.355	0.0853	2.671	1.991	1.087	1.086	SC-XRD	
Cr$_2$GeC	4.101	0.0845	2.631	1.988	1.153	1.122	XRD	[32]
Cr$_2$AlC	4.478	0.0865	2.669	1.990	1.048	1.072	XRD	
	4.480	0.0855	2.681	1.984	1.058	1.068	XRD	[44]
V$_2$AlC	4.501	0.0856	2.732	2.020	1.053	1.0653	SC-XRD	[34]
Ti$_2$AlC	4.461	0.0850	2.861	2.112	1.067	1.072	EXAFS	[27]
Nb$_2$AlC	4.471	0.0883	2.874	2.172	1.031	1.081	EXAFS	
Hf$_2$AlC	4.204	0.0877	2.928	2.244	1.094	1.108	XRD	[37]
Zr$_2$AlC	4.384	0.0871	3.052	2.301	1.061	1.089	XRD	[9]
	4.379	0.0898	3.020	2.322	1.034	1.101	NPD	
Zr$_2$SnC	4.359	0.0860	3.076	2.304	1.078	1.088	XRD	[2]
	4.341	0.0857	3.083	2.308	1.085	1.090	XRD	This work
	4.337	0.0861	3.076	2.310	1.082	1.092	NPD	

Table 2. Experimentally determined crystallographic parameters of some ternary M$_2$AC phases. The atomic distances and distortions are calculated according to Eqs (1–4).

Similarly, a parameter is defined for the distortion of the trigonal prism, p_d, which is expressed as the ratio of the distance between the M-atoms in the basal plane, $d_{M-M}(d_{M-M} = a)$, and the distance between M- and A-atoms, d_{M-A}[28,29]. The latter can be calculated from the projections in Fig. 6c, and corresponds to:

$$d_{M-A} = \sqrt{\frac{a^2}{3} + c^2\left(\frac{1}{4} - z_M\right)^2} \tag{3}$$

The distortion of the trigonal prism can be calculated as follows[28,29]:

$$p_d = \frac{d_{M-M}}{d_{M-A}} = \frac{1}{\sqrt{\frac{1}{3} + \left(\frac{1}{4} - z_M\right)^2 (c/a)^2}} \tag{4}$$

Similar to o_d, p_d equals 1 for an ideal packing of hard spheres and depends only on the crystallographic parameters c/a and z_M. Commonly, $p_d > 1$ pd, which corresponds to a compression along the c-axis as well.

These distortion parameters have been used in density functional theory (DFT) calculations to determine the free crystallographic parameters. Kanoun *et al.* calculated the effect of the A-element in Zr$_2$AC, reporting that distortions o_d and p_d increased with the number of valence electrons and with the trigonal prism becoming more strongly affected[30]. Moreover, they studied the effect of the M-element in M$_2$SnC with M = Ti, Zr, Hf and Nb, reporting a lower distortion for the octahedral block of Zr$_2$SnC and Hf$_2$SnC, as compared to the Ti- and Nb-containing M$_2$SnC. They reported this difference as a 'steric effect' and correlated it with the size of the M-atom[31]. Also Horlait *et al.* suggested a kind of steric effect in terms of the a- and c-ranges in which these 211 structures might be stable[11]. This suggestion is based on the earlier observation that the A-element mainly alters the a-LP, hence, modifying the c/a ratio.

Coming back to the distortion parameters, the A-element also modifies o_d and p_d. Therefore, it is interesting to see how these distortion parameters vary with varying solute content in the studied solid solutions. One of the main challenges to quantify these parameters, however, is the limited availability of accurate, experimentally measured literature data on z_M. Some experimentally obtained c/a and z_M values for ternary MAX phases are listed in Table 2, together with the calculated crystallographic parameters according to Eqs (1–4).

In order to estimate o_d and p_d for solid solutions, one must differentiate between the effect of M- and A-site solid solutions. Hug *et al.* determined the z_M of Ti and Nb in the M-site solid solution (Ti$_{0.5}$, Nb$_{0.5}$)$_2$AlC, using extended X-ray absorption fine structures (EXAFS). They noticed a different atomic position for Ti and Nb with z_{Ti} and z_{Nb} values close to those observed for Ti$_2$AlC and Nb$_2$AlC, respectively[27]. This suggests that the addition/substitution of an M-element only modifies slightly the atomic position of the host M-element.

With respect to A-site solid solutions, Cabioc'h *et al.* determined z_{Cr} in Cr$_2$(Al, Ge)C using XRD. Notwithstanding the large statistical error, they reported a linear trend for the evolution of z_{Cr} between Cr$_2$AlC and Cr$_2$GeC. Concomitant with a linear evolution of the a and c LPs, following Vegard's law, a gradual decrease of o_d and p_d was observed with increasing Al-content[32]. A similar correlation can be established for z_V combining the reports of Etzkorn *et al.*, who determined the LPs of V$_2$(Al$_{1-y}$, Ga$_y$)C with $1 \geq y \geq 0.43$, using single crystal X-ray diffraction (SC-XRD)[33,34]. These reports indicate that the distortion parameters can be tuned by modifying the composition of the MAX phase, especially on the A-site.

Following this reasoning, the crystallographic parameters of Zr$_2$SnC are of particular interest, as they can be used in combination with the z_M value for Zr$_2$AlC to estimate the distortion parameters for Zr$_2$(Al, Sn)C. Jeitschko *et al.* reported on the experimentally obtained a and c values and gave a generic value for z_M, valid for most reported H-phases[2]. Barsoum *et al.* reported on the experimentally obtained a and c values for M-Sn-C
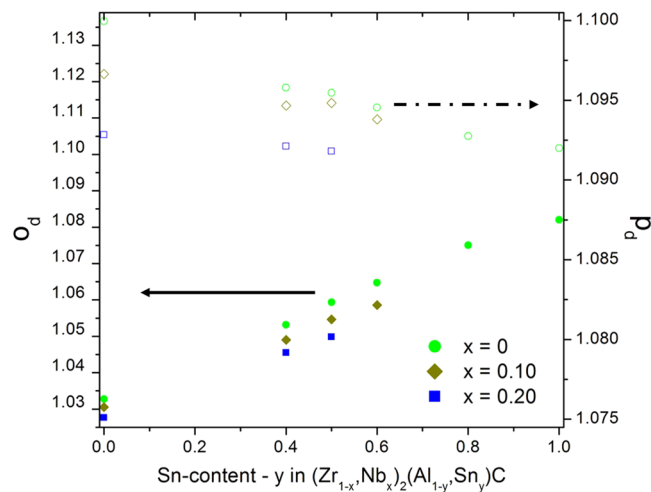
Figure 7. The distortion parameters o_d (solid symbols) and p_d (open symbols) as a function of the Sn-content for solid solutions with variable Nb-content.

phases, but no information on z_{zr} was included[17]. In order to have a reliable and direct comparison with the z_{zr} value for Zr_2AlC[9], neutron diffraction analysis was performed on Zr_2SnC powder (the refined pattern is included in the Supporting Information). This characterization technique is more precise in determining the crystallographic structure; therefore, the crystallographic parameters, especially z_M, are considered to be more accurate. The neutron diffraction data of c/a and z_{Zr} are included in Table 2. They are in good agreement with the XRD values obtained in this study and differ only slightly from the data reported by Jeitschko *et al.*[2]. Moreover, all three data sets for Zr_2SnC show a similar trend in comparison with Zr_2AlC, i.e., both c/a and z_{Zr} decreased. The calculated distortion parameters for the octahedral blocks and trigonal prisms are included in Table 2.

Of particular interest are the values for Zr_2AlC. The distortion of the trigonal prism for this compound is significantly larger than for most other M_2AC (except for Hf_2AlC). Replacing Al by Sn lowers the p_d, as can be concluded from the NPD results of Zr_2SnC. The decreased z_M was more determining than the decreased c/a–ratio. Moreover, replacing Zr with Nb also caused a decrease in p_d, as z_M is lower in Nb_2AlC and the c/a-ratio is larger (based on the EXAFS results in[27]).

Based on the preceding discussion, it finally becomes possible to combine these values for the ternary compounds with the above mentioned trends observed in M- and A-site solid solution formation. The z_M values for the solid solutions are assumed to be a linear interpolation of the ternary end-members listed in Table 2. The trends for the distortion parameters of the $(Zr, Nb)_2(Al, Sn)C$ double solid solution are illustrated in Fig. 7. Overall, the double solid solutions are characterised by a smaller distortion of the trigonal prism as compared to Zr_2AlC. Both substituting elements, Nb and Sn, contribute to a reduction in p_d. On the other hand, o_d increases significantly with increasing Sn-content, whereas Nb does not alter significantly the octahedral distortion. This analysis of the distortion parameters can be extended to the other values obtained for M_2AC phases in Table 2. Before further evaluating these numbers, it should be emphasised that the c/a and z_M data were determined with different characterization techniques and were collected from different published works. Therefore, a direct comparison is neither ideal nor recommended. Nevertheless, in the absence of a set of consistently measured z_M data for M_2AC phases, the available values can provide a first insight into the issue at hand.

With respect to the values in Table 2, Cr_2GeC has clearly the largest distortions for both building blocks. This is mainly due to the small c/a ratio of this MAX phase compound, as the distortions increase with decreasing c/a, according to Eqs (2–4). The low z_M value is the reason why $o_d > p_d$, as the former is inversely proportional to z_M, whereas the latter scales with the z-coordinate of the M-atom. Considering these large distortion parameters for Cr_2GeC, a stable M_2AC compound, we are not able to specify a range of numbers associated with crystal geometry that unambiguously determines phase stability.

However, the distortion of the trigonal prism is an interesting case, as it serves as a measure for the steric match between M- and A-elements, where $p_d = 1$ means that M and A are identical. From that perspective, and in accordance with Hägg's rule for binary carbides, it is worthwhile comparing the atomic radii of different M- and A-elements. An overview of Goldschmidt's atomic diameter[35] plotted as function of electronegativity is given in Fig. 8. For M_2AlC compounds, the largest p_d-values are found for Zr and Hf, which have similar atomic radii, and are the two largest M-atoms, outsized only by the rare-earth elements Sc and Y (Fig. 8a). On the other hand, Al is one of the smaller A-atoms based on Fig. 8b. Therefore, a large p_d value can be interpreted as a large steric mismatch associated with differences in the size (atomic radii) of the M- and A-elements.

A steric point of view on the reported, experimentally synthesized M_2AC structures is obtained when the atomic radii of the M-elements are plotted versus the radii of the A-elements (from groups 13 and 14). This elementary plot is shown in Fig. 9a. It appears that, overall, large M-atoms preferentially combine with large A-atoms, and the same holds for the small M- and A-elements. This possibly explains why certain M/A combinations are not observed experimentally. However, some outlier combinations have been reported, i.e., Zr_2AlC,
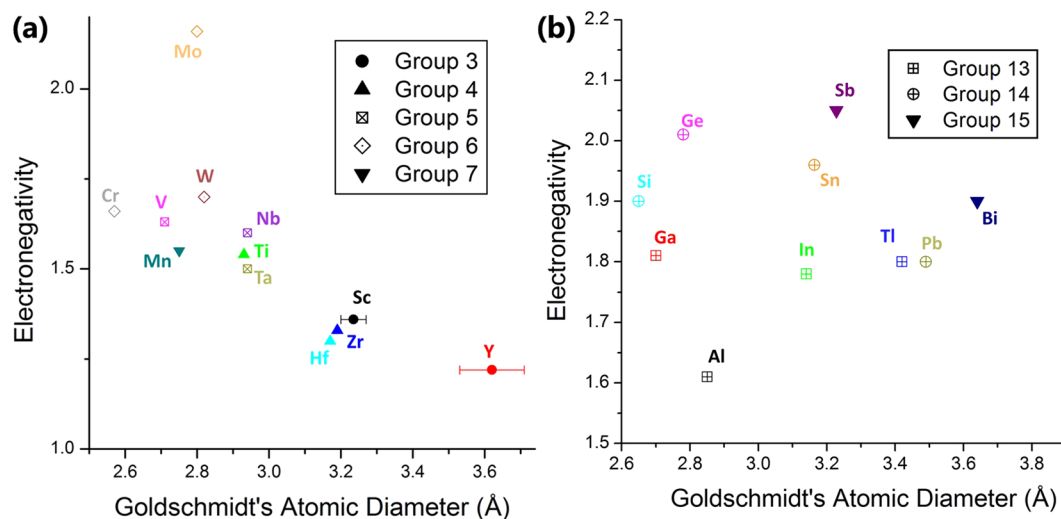
Figure 8. Goldschmidt's atomic diameter vs. electronegativity for different (**a**) M-metals and (**b**) metallic A-elements. The atomic diameter data were obtained from[35].
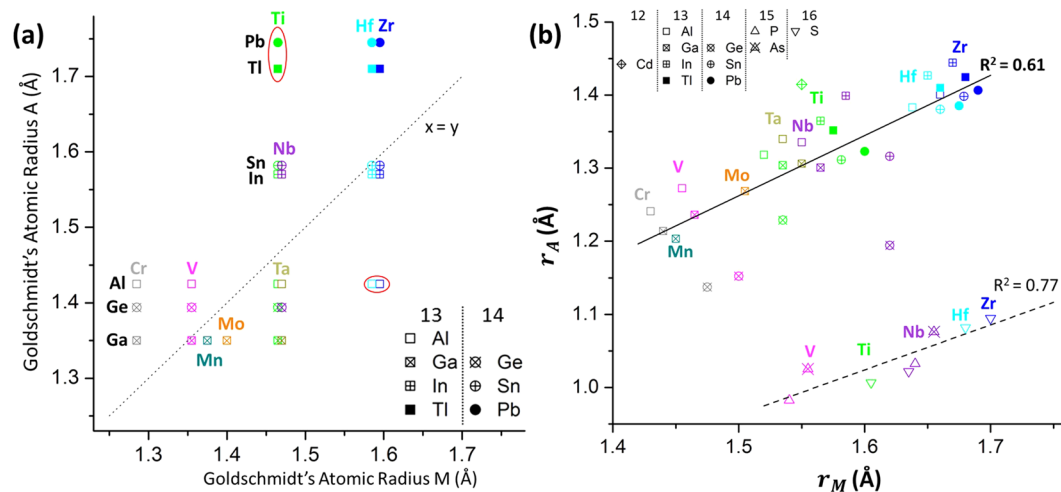
Figure 9. Comparison of the atomic radii of the M- and A-elements in M_2AC MAX phases, based on (**a**) Goldschmidt's atomic radii, and (**b**) the radii values determined by Eqs (5) and (6). The red ellipses indicate the outliers discussed in the text.

Hf_2AlC, Ti_2PbC and Ti_2TlC (indicated by red ellipses in Fig. 9a). These phases can be regarded on the cusp of steric stability. MAX phases in the Zr-Al-C and Hf-Al-C systems combine a large M-atom with a small A-atom. They have been only recently experimentally synthesised[9,36,37], always in combination with MC binary carbides and never as phase-pure bulk compounds. This might be associated with the aforementioned steric effect and their outlier positions in Fig. 9a. A similar comment can be given for both Ti_2PbC and Ti_2TlC, which combine a small M-atom with a large A-atom. These compounds were discovered by Jeitschko *et al.* in 1964 and diverted significantly from the conventional H-phase structure. A first oddity is the value of z_{Ti} in these compounds, as it was specifically discussed and lowered to 0.08 instead of 0.086 for the other H-phases. Moreover, the Pb-defect structure for Ti_2PbC was described as '$(Ti_{1.97}, Pb_{0.03})_2(Pb_{0.9}, Ti_{0.03})C_{1-x}$' and a similar structure was assumed for the Tl-containing equivalent (*Ähnliches gilt auch für die Phase Ti_2TlC*)[38]. Curiously, no other reports on these H-phases (members of the MAX phase family) were found thereafter.

Figure 9b is an alternative plot for all 40 M_2AC phases, which shows the atomic radii of M (r_M) versus the atomic radii of A (r_A), based on their size in the MAX phase lattice, with:

$$r_M = \frac{a}{2} \tag{5}$$

and

$$r_A = d_{M-A} - r_M = \sqrt{\frac{a^2}{3} + c^2\left(\frac{1}{4} - z_M\right)^2} - \frac{a}{2}$$

(6)

where z_M is generically chosen equal to 0.086. In Fig. 9b, two groups can be clearly distinguished. The points in the lower part of the plot correspond to the 7 MAX phases based on P, S and As, whereas the points in the upper plot part correspond to the other 33 M_2AC MAX phases. For both groups, a linear correlation between r_M and r_A can be postulated, where the values for r_M are in general larger than r_A. The significantly smaller r_A for the MAX phases containing elements from groups 15 and 16 (non-metallic and metalloid elements) is attributed to their small c/a ratio. The latter might be related with the large electronegativity value of P (2.19), S (2.58) and As (2.18), as compared to the metallic A-elements (cf. Fig. 8b). The deviatory behaviour of S, and to a lesser extend of As, was also noticed by Barsoum when plotting the number of valence electrons (n_{val}) versus the theoretical density of states at the Fermi level (N(E_f))[29]. No P-containing phases were included there. One additional remark, the atomic radii for the MAX phases containing the metalloid Ge (2.01) are found between the two linear trends, indicating that the non-metal/metal transition of the periodic table can also be observed in the MAX phase structure.

Coming back to the initial impetus of this work, i.e., the synthesis of a phase-pure Zr_2AlC-based MAX phase solid solution, one can interpret the effect of the different solute atoms in a steric way. The addition of Nb reduces the size of the average M-atom, whereas the addition of Sn increases the average size of the A-atom. In this way, the additives reduce the steric mismatch in the trigonal prism. This suggestion closely relates with one of the guidelines for solid solution formation in metallic alloys, formulated by Hume-Rothery[35]. This steric interpretation also provides an explanation for the trend that Horlait et al. observed for $Zr_2(Al, A)C$ solid solutions, i.e., that solute elements larger than Al, i.e., Sn, Pb, Sb and Bi, facilitated the formation of the Zr-containing 211 MAX phase[11,16].

The Hume-Rothery atomic radii rule also holds for most reported $(M, M')_{n+1}AC_n$ and $M_{n+1}(A, A')C_n$ solid solutions, where a more limited solubility is observed with increasing difference in atomic radii[13,39,40]. As case study, the literature on Cr_2AC-based MAX phases is investigated, with Cr the smallest M-element, in contrast to Zr that is the largest M-element according to Fig. 8b. The three ternary systems experimentally reported are Cr_2AlC, Cr_2GeC and Cr_2GaC. These A-elements are small atoms that can replace each other resulting in the reported solid solutions $Cr_2(Al, Ge)C$[32] and $Cr_2(Al, Ga)C$[33], in agreement with the Hume-Rothery rule. A third solid solution is reported, i.e., $Cr_2(Al, Si)C$[41]. Even though no ternary M_2SiX phase exists to the best of our knowledge, the only 211 structured solid solution containing Si, the smallest reported A-element according to Fig. 8b, forms in combination with Cr, the smallest reported M-atom.

An additional remark with respect to the atomic radius match is that when M/A and M'/A' differ significantly, substitution might be very limited or, alternatively, in-plane ordering of the atoms might occur. The latter is illustrated by the recently synthesised, in-plane ordered 211 "i-MAX" phases, i.e., $(Mo_{2/3}, Sc_{1/3})_2AlC$, $(V_{2/3}, Zr_{1/3})_2AlC$, $(Cr_{2/3}, Sc_{1/3})_2AlC$, $(Cr_{2/3}, Y_{1/3})_2AlC$ and $(Mo_{2/3}, Y_{1/3})_2AlC$[15,42,43], where M:M' = 2:1 and the atomic radius of M is substantially smaller than that of M' (see Fig. 8a).

To conclude this section, there seems to be a steric effect present in the M_2AC structure that can be used to improve the stability and phase purity of certain M-A-C combinations. The proposed rule of thumb implicates the partial substitution of the M- and/or A-element with an element that is appropriate in terms of atomic radius. A good match between the atomic radii of M and A should be targeted in agreement with the graphs of Fig. 8. In order to further validate this suggestion, however, more data on experimentally obtained solid solutions are required. In a second step, it would be possible to further elaborate the correlation of phase stability with the lattice distortion parameters. In order to do so, accurately determined z_M parameters for the various ternary and quaternary MAX phase systems are required.

Conclusions

The possibility to stabilize Zr_2AlC and to eliminate parasitic ZrC formation by the addition of Nb and/or Sn was investigated. The two quaternary systems $(Zr, Nb)_2AlC$ and $Zr_2(Al, Sn)C$ were found to be stable over their entire compositional range and both Nb and Sn promoted the formation of the 211 MAX phase. Sn is preferred over Nb, as it is selectively incorporated into the MAX phase structure, whereas Nb is also observed in most competing phases, i.e., $(Zr, Nb)C$, $(Zr, Nb)Al_2$ and $(Nb, Zr)Al_3$. The lattice parameters (LPs) a and c were determined by XRD for both solid solutions and obeyed Vegard's law. The addition of Nb significantly lowered both LPs, whereas the substitution of Al with Sn mainly increased the a-LP and left c practically unaffected. A similar trend was observed for the a- and c-parameters of the $(Zr, Nb)_2(Al, Sn)C$ double solid solution. A nearly single-phase 211 MAX material was obtained with a Zr:Nb ratio of 80:20 and Al:Sn ratio of 50:50, for which the rock-salt-like (Zr, Nb)C phase was eliminated. Moreover, an M:A ratio starting powder composition of 2:1.05 was used to minimize the amount of the $ZrAl_2$ phase.

The effect of Nb and Sn on the crystallographic parameters was studied in detail. Neutron powder diffraction of Zr_2SnC was performed to accurately determine the z-coordinate of Zr in the 211 unit cell. This analysis showed that the prismatic distortion in Zr_2AlC is significantly larger than the octahedral distortion, and that the former can be reduced by the addition of Nb and Sn. The addition of Sn increased the octahedral distortion.

The analysis was expanded and the general crystallographic structure of the 211 MAX phase carbides was discussed. No phase stability range could be determined in terms of distortion parameters, but a correlation between the atomic radii of the M and A elements was proposed. The large M-atoms combine notably better with large A-atoms and the small M-atoms with small A-atoms. This match in atomic radii between M and A can be used as a practical guideline for the synthesis of other MAX phase solid solutions. In general, the concept of a double solid solution was found advantageous in terms of MAX phase synthesis and MAX phase purity.

References

1. Barsoum, M. W. & El-Raghy, T. Synthesis and Characterization of a Remarkable Ceramic: Ti$_3$SiC$_2$. *J. Am. Ceram. Soc.* **79**, 1953–1956, https://doi.org/10.1111/j.1151-2916.1996.tb08018.x (1996).
2. Jeitschko, W., Nowotny, H. & Benesovsky, F. Kohlenstoffhaltige ternäre Phasen (H-Phase). *Monatshefte für Chemie* **94**, 672–676 (1963).
3. Barsoum, M. W. & El-Raghy, T. The MAX phases: Unique new carbide and nitride materials - Ternary ceramics turn out to be surprisingly soft and machinable, yet also heat-tolerant, strong and lightweight. *Am. Scientist* **89**, 334–343, https://doi.org/10.1511/2001.28.736 (2001).
4. Barsoum, M. W. The M$_{n+1}$AX$_n$ phases: A new class of solids: Thermodynamically stable nanolaminates. *Progress in Solid State Chemistry* **28**, 201–281, https://doi.org/10.1016/S0079-6786(00)00006-6 (2000).
5. Grove, C., Shepherd, D., Thomas, M. & Little, P. Neutronics of MAX phase materials. *Proceedings SMINS-4, 11–14 July* 2016, *Manchester, UK*, 1–14 (2016).
6. Lambrinou, K. *et al*. In *Water React. Fuel Perform. Meet.*, *Jeju Island, Korea* (2017).
7. Utili, M., Agostini, M., Coccoluto, G. & Lorenzini, E. Ti$_3$SiC$_2$ as a candidate material for lead cooled fast reactor. *Nuclear Engineering and Design* **241**, 1295–1300, https://doi.org/10.1016/j.nucengdes.2010.07.038 (2011).
8. Müller, G. *et al*. Results of steel corrosion tests in flowing liquid Pb/Bi at 420–600 °C after 2000 h. *Journal of Nuclear Materials* **301**, 40–46, https://doi.org/10.1016/S0022-3115(01)00725-5 (2002).
9. Lapauw, T. *et al*. Synthesis of the new MAX phase Zr$_2$AlC. *Journal of the European Ceramic Society* **36**, 1847–1853, https://doi.org/10.1016/j.jeurceramsoc.2016.02.044 (2016).
10. Lambrinou, K., Lapauw, T., Tunca, B. & Vleugels, J. In *Developments in Strategic Ceramic Materials II* 223–233 (John Wiley & Sons, Inc., 2017).
11. Horlait, D., Grasso, S., Chroneos, A. & Lee, W. E. Attempts to synthesise quaternary MAX phases (Zr, M)$_2$AlC and Zr$_2$(Al, A)C as a way to approach Zr$_2$AlC. *Materials Research Letters*, 1-8, https://doi.org/10.1080/21663831.2016.1143053 (2016).
12. Reiffenstein, E., Nowotny, H. & Benesovsky, F. Strukturchemische und magnetochemische Untersuchungen an Komplexcarbiden. *Monatsh für Chem verw Teile anderer Wiss* **97**, 1428–1436 (1966).
13. Naguib, M. *et al*. New Solid Solution MAX Phases: (Ti$_{0.5}$, V$_{0.5}$)$_3$AlC$_2$, (Nb$_{0.5}$, V$_{0.5}$)$_2$AlC, (Nb$_{0.5}$, V$_{0.5}$)$_4$AlC$_3$ and (Nb$_{0.8}$, Zr$_{0.2}$)$_2$AlC. *Materials Research Letters* **2**, 233–240, https://doi.org/10.1080/21663831.2014.932858 (2014).
14. Tunca, B. *et al*. Synthesis of MAX Phases in the Zr-Ti-Al-C System. *Inorganic Chemistry* **56**, 3489–3498, https://doi.org/10.1021/acs.inorgchem.6b03057 (2017).
15. Dahlqvist, M. *et al*. Prediction and synthesis of a family of atomic laminate phases with Kagomé-like and in-plane chemical ordering. *Science Advances* **3**, https://doi.org/10.1126/sciadv.1700642 (2017).
16. Horlait, D., Middleburgh, S. C., Chroneos, A. & Lee, W. E. Synthesis and DFT investigation of new bismuth-containing MAX phases. *Scientific Reports* **6**, 18829, https://doi.org/10.1038/srep18829 (2016).
17. Barsoum, M. W., Yaroschuk, G. & Tyagi, S. Fabrication and characterization of M$_2$SnC (M = Ti, Zr, Hf and Nb). *Scr. Mater.* **37**, 1583–1591, https://doi.org/10.1016/s1359-6462(97)00288-1 (1997).
18. Salama, I., El-Raghy, T. & Barsoum, M. W. Synthesis and mechanical properties of Nb$_2$AlC and (Ti, Nb)$_2$AlC. *Journal of Alloys and Compounds* **347**, 271–278, https://doi.org/10.1016/S0925-8388(02)00756-9 (2002).
19. Lutterotti, L., Matthies, S. & Wenk, H. MAUD: a friendly Java program for material analysis using diffraction. *Newsletter of the CPD* **21**, 14–15 (1999).
20. Popa, N. The (hkl) dependence of diffraction-line broadening caused by strain and size for all Laue groups in Rietveld refinement. *Journal of Applied Crystallography* **31**, 176–180 (1998).
21. Rivin, O., Caspi, E. N., Ettedgui, H., Shaked, H. & Gukasov, A. Magnetic structure determination of TbCo$_2$Ni$_3$ using polarized and nonpolarized neutron powder diffraction. *Physical Review B* **88**, 054430 (2013).
22. Gusev, A. I. Phase diagrams of the pseudobinary TiC-NbC, TiC-TaC, ZrC-NbC, ZrC-TaC, and HfC-TaC carbide systems. *Russian Journal of Physical Chemistry* **59**, 336–340 (1985).
23. Rokhlin, L. & Bochvar, N. In *Light Metal Systems. Part 3: Selected Systems from Al-Fe-V to Al-Ni-Zr.* (eds Effenberg, G. & Ilyenko, S.) 1–9 (Springer Berlin Heidelberg, 2005).
24. Lapauw, T. *et al*. (Nb$_x$, Zr$_{1−x}$)$_4$AlC$_3$ MAX Phase Solid Solutions: Processing, Mechanical Properties, and Density Functional Theory Calculations. *Inorganic Chemistry* **55**, 5445–5452, https://doi.org/10.1021/acs.inorgchem.6b00484 (2016).
25. Zheng, L., Wang, J. & Zhou, Y. Improving the High-Temperature Oxidation Resistance of Nb$_4$AlC$_3$ by Silicon Pack Cementation. *J. Am. Ceram. Soc.* **97**, 552–561, https://doi.org/10.1111/jace.12667 (2014).
26. Hägg. *Zeitschrift für Kristallographie, Kristallgeometrie, Kristallphysik, Kristallchemie* **89**, 92 (1934).
27. Hug, G., Jaouen, M. & Barsoum, M. W. X-ray absorption spectroscopy, EELS, and full-potential augmented plane wave study of the electronic structure of Ti$_2$AlC, Ti$_2$AlN, Nb$_2$AlC, and (Ti$_{0.5}$ Nb$_{0.5}$)$_2$AlC. *Physical Review B* **71**, 024105 (2005).
28. Hug, G. Electronic structures of and composition gaps among the ternary carbides Ti$_2$MC. *Physical Review B* **74**, 184113 (2006).
29. Barsoum, M. W. *MAX Phases: Properties of Machinable Ternary Carbides and Nitrides.* (Wiley-VCH Verlag GmbH & Co., 2013).
30. Kanoun, M. B., Goumri-Said, S., Reshak, A. H. & Merad, A. E. Electro-structural correlations, elastic and optical properties among the nanolaminated ternary carbides Zr$_2$AC. *Solid State Sciences* **12**, 887–898, https://doi.org/10.1016/j.solidstatesciences.2010.01.035 (2010).
31. Kanoun, M. B., Goumri-Said, S. & Reshak, A. H. Theoretical study of mechanical, electronic, chemical bonding and optical properties of Ti$_2$SnC, Zr$_2$SnC, Hf$_2$SnC and Nb$_2$SnC. *Computational Materials Science* **47**, 491–500, https://doi.org/10.1016/j.commatsci.2009.09.015 (2009).
32. Cabioc'h, T., Eklund, P., Mauchamp, V., Jaouen, M. & Barsoum, M. W. Tailoring of the thermal expansion of Cr$_2$(Al$_x$, Ge$_{1−x}$)C phases. *Journal of the European Ceramic Society* **33**, 897–904, https://doi.org/10.1016/j.jeurceramsoc.2012.10.008 (2013).
33. Etzkorn, J., Ade, M., Kotzott, D., Kleczek, M. & Hillebrecht, H. Ti$_2$GaC, Ti$_4$GaC$_3$ and Cr$_2$GaC—Synthesis, crystal growth and structure analysis of Ga-containing MAX-phases M$_{n+1}$GaC$_n$ with M = Ti, Cr and n = 1, 3. *Journal of Solid State Chemistry* **182**, 995–1002, https://doi.org/10.1016/j.jssc.2009.01.003 (2009).
34. Etzkorn, J., Ade, M. & Hillebrecht, H. V$_2$AlC, V$_4$AlC$_{3−x}$ (x ≈ 0.31), and V$_{12}$Al$_3$C$_8$: Synthesis, Crystal Growth, Structure, and Superstructure. *Inorganic Chemistry* **46**, 7646–7653, https://doi.org/10.1021/ic700382y (2007).
35. Hume-Rothery, W. *The Structure of Metals and Alloys.* 137 (The Institute of Metals, London, 1950).
36. Lapauw, T. *et al*. Synthesis of MAX Phases in the Hf–Al–C System. *Inorganic Chemistry* **55**, 10922–10927, https://doi.org/10.1021/acs.inorgchem.6b01398 (2016).
37. Lapauw, T. *et al*. Synthesis of the novel Zr$_3$AlC$_2$ MAX phase. *Journal of the European Ceramic Society* **36**, 943–947, https://doi.org/10.1016/j.jeurceramsoc.2015.10.011 (2016).
38. Jeitschko, W., Nowotny, H. & Benesovsky, F. Die H-Phasen Ti$_2$TlC, Ti$_2$PbC, Nb$_2$InC, Nb$_2$SnC und Ta$_2$GaC. *Monatshefte für Chemie und verwandte Teile anderer Wissenschaften* **95**, 431–435, https://doi.org/10.1007/BF00901306 (1964).
39. Lapauw, T., Swarnakar, A. K., Tunca, B., Lambrinou, K. & Vleugels, J. Nanolaminated ternary carbide (MAX phase) materials for high temperature applications. *International Journal of Refractory Metals and Hard Materials* **72**, 51–55, https://doi.org/10.1016/j.ijrmhm.2017.11.038 (2018).
40. Schuster, J., Nowotny, H. & Vaccaro, C. The ternary systems: Cr-Al-C, V-Al-C, and Ti-Al-C and the behavior of H-phases (M$_2$AlC). *Journal of Solid State Chemistry* **32**, 213–219 (1980).

41. Yu, W., Li, S. & Sloof, W. G. Microstructure and mechanical properties of a Cr$_2$Al(Si)C solid solution. *Materials Science and Engineering: A* **527**, 5997–6001 (2010).
42. Tao, Q. *et al.* Two-dimensional Mo$_{(1.33)}$C MXene with divacancy ordering prepared from parent 3D laminate with in-plane chemical ordering. *Nature Communications* **8**, 14949, https://doi.org/10.1038/ncomms14949 (2017).
43. Lu, J. *et al.* Theoretical and Experimental Exploration of a Novel In-Plane Chemically Ordered (Cr$_{2/3}$M$_{1/3}$)$_2$AlC i-MAX Phase with M = Sc and Y. *Crystal Growth & Design* **17**, 5704–5711, https://doi.org/10.1021/acs.cgd.7b00642 (2017).
44. Jaouen, M., Chartier, P., Cabioc'h, T., Mauchamp, V., André, G. & Viret, M. Invar like behavior of the Cr$_2$AlC MAX phase at low temperature. *Journal of the American Ceramic Society* **96**, 3872–3876 (2013).

Acknowledgements

Author Contributions

T.L. main author, conducted most of the experiments. B.T. co-author, assisted in experimental part. D.P. conducted neutron powder diffraction experiments. A.P. & O.O. conduction/supervision of neutron powder diffraction experiments, revision of manuscript. J.V. & K.L. guidance of scientific work, revision of manuscript.

Additional Information

Supplementary information accompanies this paper at https://doi.org/10.1038/s41598-018-31271-2.

Competing Interests: The authors declare no competing interests.

Publisher's note: Springer Nature remains neutral with regard to jurisdictional claims in published maps and institutional affiliations.